THE JOURNAL OF PHYSICAL CHEMISTRY Letters

Letter

pubs.acs.org/JPCL

Thermoactivated Electrical Conductivity in Perylene Diimide Nanofiber Materials

Na Wu,[†] Yaqiong Zhang,[†] Chen Wang,[†] Paul M. Slattum,[‡,§] Xiaomei Yang,[†] and Ling Zang*[,†]

[†]Nano Institute of Utah and Department of Materials Science and Engineering, University of Utah, 36 South Wasatch Drive, Salt Lake City, Utah 84112, United States

[‡]Vaporsens Inc., 36 South Wasatch Drive, Salt Lake City, Utah 84112, United States

[§]Leibniz-Institut für Polymerforschung Dresden e.V., Hohe Straße 6, D-01069 Dresden, Germany

Supporting Information

ABSTRACT: Thermoactivated electrical conductivity has been studied on nanofibers fabricated from the derivatives of perylene tetracarboxylic diimide (PTCDI) both in the dark and under visible light illumination. The activation energy obtained for the nanofibers fabricated from donor−acceptor (D−A) PTCDIs are higher than that for symmetric *n*-dodecyl substituted PTCDI. Such difference originates from the strong dependence of thermoactivated charge hopping on material disorder, which herein is dominated by the D−A charge-transfer and dipole−dipole interactions between stacked molecules. When the nanofibers were heated above the first phase transition temperature (around 85 °C), the activation energy was significantly increased because of the thermally enhanced polaronic effect. Moreover, charge carrier density can be increased in the D−A nanofibers under visible light illumination. Consistent with the theoretical models in the literature, the increased charge carrier density did cause decrease in the activation energy due to the up-shifting of Fermi level closer to the conduction band edge.

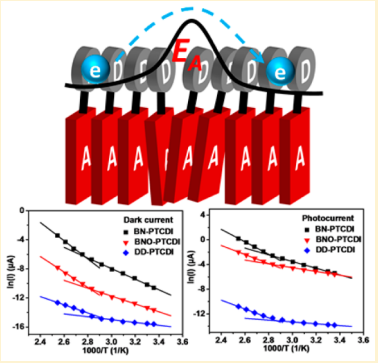

Organic semiconductor materials have drawn increasing attention in both fundamental and applied research, mainly because of the unique features of these materials in comparison to those of conventional inorganic counterparts.[1−4] The typical features include structure and property flexibility through molecular design and engineering, low-temperature solution processability, and mechanical conformity to different shapes of substrate. Organic semiconductors have been employed in a wide variety of electronic and optoelectronic devices, such as transistors, diodes, sensors, solar cells, and light-emitting devices. The operation performance of these device systems is usually highly concerned with the electrical conductivity (or the charge transport) within the materials. Although the electrical conductivity of the organic semiconductor is primarily determined by the intrinsic structure (e.g., molecular structure, intermolecular arrangement), some extrinsic physical parameters like temperature can also cause significant modulation in the conductivity through changing the carrier mobility via the so-called thermoactivated process. With this sensitive temperature dependence, some organic materials have been developed into temperature sensors,[5−7] which are suited for integration into wearable systems for in situ monitoring of human activity and personal healthcare.[8−10]

In general, the charge transport in organic materials relies on hopping between the localized energy states (trapped charges),[11−13] which can typically be described as a thermoactivated process. Higher temperatures facilitate transport by providing the thermo-energy required to overcome the energetic barriers created by disorders. Arrhenius fitting of the conductivity as a function of temperature gives estimation of the activation energy. For many organic semiconductors (including conducting polymers), the activation energy was determined in the range of tens to hundreds of millielectronvolts.[13−15] The origin of the activation energy can be attributed to two major contributions: the energetic disorder and the polaronic effect.[13,16] The former is usually referred to the diagonal disorder, which is referred to the fluctuations in molecular electronic energies as arranged within the material. Such energetic disorder is commonly described as a Gaussian distribution of the molecular electronic energies [mostly the highest occupied molecular orbital (HOMO) and lowest unoccupied molecular orbital (LUMO) level energies], which is usually referred as the Gaussian disorder model (GDM).[16] While the diagonal disorder is mainly contributed by the conformational freedom of component molecules, it can also be induced by electrostatic or polarization effects from surrounding molecules, particularly when the molecules contain significant dipole moments (e.g., the electron donor−acceptor structure).[17,18] The polaronic effect in organic materials is mainly due to molecular distortion caused by charging and decharging a molecule with an electron.[16,19,20] Hopping of an electron, in this case, is associated with both intramolecular and intermolecular reorganization in solid stacks. It is evidenced that the polaronic effect can become more significant at

Received: November 10, 2016
Accepted: December 19, 2016
Published: December 19, 2016

DOI: 10.1021/acs.jpclett.6b02639
J. Phys. Chem. Lett. 2017, 8, 292−298

elevated temperature because of the increased molecular vibration.[16]

Description of charge transport considers both the charge hopping rates between the localized sites and the density of charges involved in the hopping. Some well-established models, such as the Miller−Abrahams model and that based on Marcus theory, have been developed to describe the hopping rate in disordered organic materials. With the varying densities of charges (e.g., modulated by gate voltage in field-effect transistors, or chemical doping through electron donor or acceptor modification), these theoretical models have been successfully applied in interpreting the observed temperature dependence of electrical conductivity of different organic materials. However, most of these studies were performed on the conducting polymers like those based on poly(*p*-phenylenevinylene) (PPV) and poly(3-hexylthiophene) (P3HT), or the intrinsic (n- or p-type) molecular semiconductor materials such as the crystals of pentacene, rubrene, or triphenylene.[13] We report therein on the temperature-activated charge transport within self-doped organic semiconductors, which were assembled from the covalently linked electron donor−acceptor (D−A) molecules based on the derivatives of perylene tetracarboxylic diimide (PTCDI, Scheme 1). As a unique air-stable n-type organic semiconductor, PTCDIs have been explored for various electrical or optical applications such as photovoltaics, light-emitting diodes, and photoelectric sensors.[1,21−23] More importantly, PTCDI materials offer robust thermal stability with decomposition temperature around 400 °C or above,[24] thus enabling investigation of thermoactivation in a wide high-temperature range.

Scheme 1. Molecular Structures of PTCDI Derivatives Studied in This Work

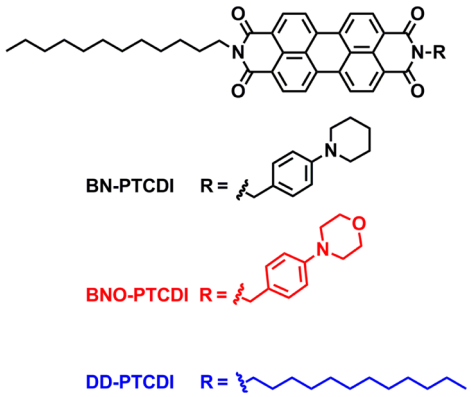

D−A molecular materials provide increased electrical conductivity through the charge-transfer interaction between the donor and acceptor moieties, which in turn results in increase in charge carrier density.[1,25−27] Because of the effective self-doping, D−A materials have been widely employed in electronic and optoelectronic systems or devices, particularly photovoltaics. Despite the gain of increased conductivity, the D−A charge transfer creates structural disorder and/or polaronic effect, which combined lead to increased energetic barrier for the charge hopping, meaning a higher temperature will be needed to activate the charge transport. It therefore becomes imperative to study the temperature-dependent charge transport of these materials. Moreover, most of the D−A materials are also photoconductive, i.e., light illumination of these materials initiates the electron transfer from D to A moiety, and further charge separation leads to increase in charge carrier density.[27] Increasing carrier density will shift up the Fermi level to the conduction band, resulting in decrease in thermoactivation energy for the charge hopping, for which the activation barrier is generally considered as the energy difference between the trapped state and conduction band.[28,29] In this regard, the photoconductive feature of D−A materials provides an alternative way to study the thermoactivated charge transport by changing the carrier density, in a manner similar to that of the studies employing field-effect transistors (FET), wherein the charge carrier density can be modulated by the gate voltage.

The PTCDI D−A materials used in this study are in the nanofiber morphology (Figure 1), which are fabricated by solution self-assembly of the D−A molecules, BN-PTCDI and BNO-PTCDI (see Supporting Information). The one-dimensional (1D) morphology is dominated by the $\pi-\pi$ stacking of the planar PTCDI molecules, and the 1D molecular stacking facilitates the charge separation between the photogenerated electron and hole through the intermolecular π-electron delocalization.[27] The further increased charge carrier density is conducive to studying the thermoactivated charge transport, for which the activation energy is related to the charge carrier density as evidenced in the FET studies. Although PTCDI nanofiber materials have been extensively studied and used in varying applications (e.g., photovoltaics, sensors), there is little research reported yet on the temperature-dependent charge transport or electrical conductivity. The presented work would fill in this research gap, by providing improved understanding of the thermoactivated charge transport, and the observation may furthermore lead to development of wearable temperature sensors, taking advantages of the flexibility and small size of the nanofibers.

Along with the two D−A molecules, BN-PTCDI and BNO-PTCDI (Scheme 1), a normal PTCDI molecule (without substitution of D moiety), DD-PTCDI, was also employed as a control in this study to investigate the effect of D−A structure and the photoinduced charge separation on the thermoactivated charge transport. While DD-PTCDI was synthesized following the same method previously reported,[30] BN-PTCDI and BNO-PTCDI were synthesized using a modified procedure as detailed in the Supporting Information. As expected, these PTCDI molecules form well-defined nanofibers when self-assembled in solutions (Figure 1a−c), mainly dictated by the strong $\pi-\pi$ stacking interaction in between. All the nanofibers are in high aspect ratio with length in the range of a few tens of micrometers. The average width of the nanofibers, as estimated by atomic force microscopy (AFM) imaging, is ca. 263, 213, and 200 nm for BN-PTCDI, BNO-PTCDI, and DD-PTCDI, respectively. These nanofibers were then deposited onto interdigitated electrodes (IDEs) for electrical measurement and characterization (Figure 1d).

For all the three PTCDI nanofibers, the electrical current measured under the same conditions (as illustrated in Figure 1d) showed significant increase with temperature when heated from 25 to 120 °C (Figure 2). One typical heating−cooling cycle, as monitored over the BN-PTCDI nanofibers, is shown in Figure S1. The temperature responses observed were completely reversible, indicating the structure robustness of PTCDI materials under heating. Such robust repeatability assures the feasibility of applying these materials in temperature sensors in the future. Among the three nanofibers, BN-PTCDI demonstrated the most sensitive dependence on temperature

DOI: 10.1021/acs.jpclett.6b02639
J. Phys. Chem. Lett. 2017, 8, 292−298

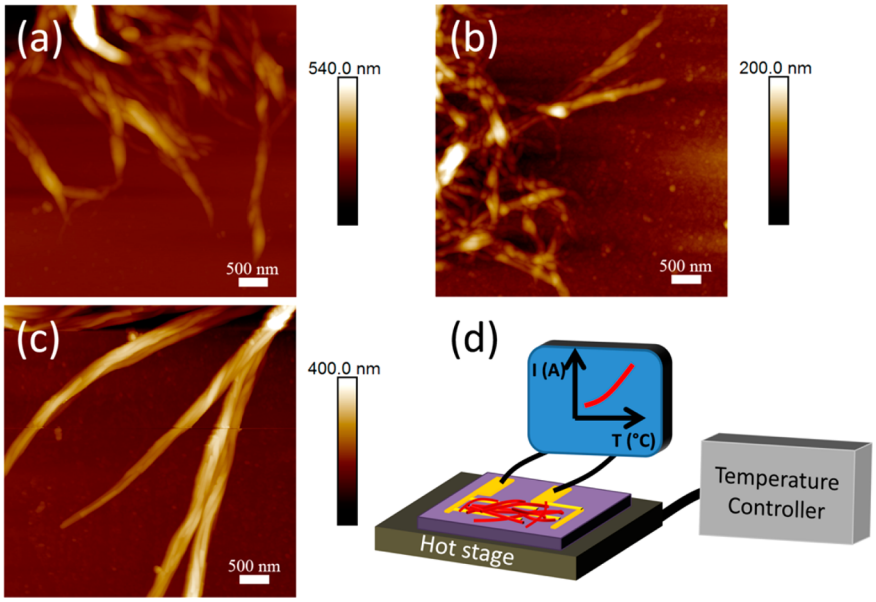

Figure 1. Tapping mode AFM topography images of (a) BN-PTCDI, (b) BNO-PTCDI, and (c) DD-PTCDI nanofibers. (d) Schematic of the IDEs device and temperature control system used for studying the thermoactivated charge transport of PTCDI nanofibers.

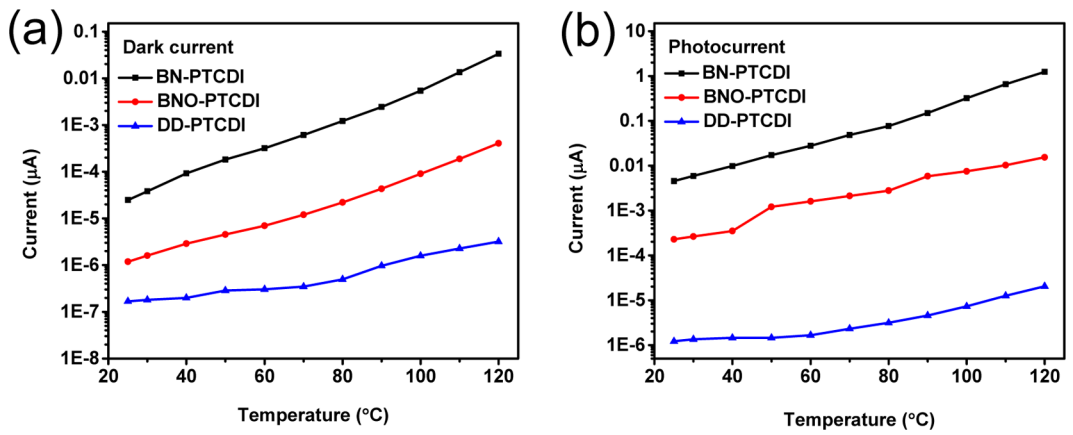

Figure 2. Electrical current of PTCDI nanofibers measured at varying temperatures in the dark (a) and under white light illumination (7.5 mW cm^{-2}) (b). A constant bias of 10 V was applied during all the measurements. The dark current of BN-PTCDI is 2 orders of magnitude higher than that of DD-PTCDI, and this is likely due to the self-doping by the piperidine group, which is a strong electron donor; a similar piperidine structure was used before for self-doping of other PTCDIs to increase the electrical conductivity.[25]

both in the dark and under white light illumination which creates photoconductivity as indicated by the much increased current. With the temperature increased from 25 to 120 °C, the current increased by a factor of 1350, 342, and 19 in the dark (Figure 2a) and 273, 67, and 17 under illumination (Figure 2b) for BN-PTCDI, BNO-PTCDI, and DD-PTCDI, respectively. Under both dark and illuminated conditions, the relative increase of current with temperature of BNO-PTCDI is significantly smaller than that of BN-PTCDI, but is still much larger than that of DD-PTCDI. The more sensitive temperature dependence of current means higher energy barrier for the thermoactivated charge transport, and this can be seen more clearly from the activation energy, which can in turn be estimated from the linear fitting of the data in Figure 2 (see Figure S2) using the Arrhenius equation (eq 1)[13,16]

$$I = I_0 e^{-E_A/kT} \quad (1)$$

where I is the electrical current measured under temperature T; k the Boltzmann constant; E_A the activation energy; and I_0 the current when E_A is ignored, i.e., in the case of free charge transport. As shown in Figure S2, good linear fitting can be obtained for the data either in the low- (25−80 °C) or high-temperature range (80−120 °C) with a turning point around 80 °C, but not in the whole temperature range of the experiment. The slope of the linear fitting gives the activation energies, E_A, which are summarized in Table 1 for comparison between the three nanofibers. The two linear ranges may indicate two different phases of the material, which would be characteristic with different activation energy. Remarkably, the turning temperature indicated in Figure S2 (80 °C) is highly consistent with the result of DSC (shown in Figure S4), wherein one phase transition temperature of 85 °C was observed for DD-PTCDI. For both the dark current and photocurrent measurements, larger activation energy was observed in the higher-temperature range for all the three nanofibers, implying that some additional contribution to the thermoactivation barrier was generated by increasing temperature. We attribute this additional contribution to the heating-

DOI: 10.1021/acs.jpclett.6b02639
J. Phys. Chem. Lett. 2017, 8, 292−298

Table 1. Activation Energy (E_A) Estimated for the Three PTCDI Nanofibers in the Low- and High-Temperature Range from Both the Dark Current and Photocurrent Measurements

	E_A in the dark (meV)		E_A under illumination (meV)	
sample	25−80 °C	80−120 °C	25−80 °C	80−120 °C
BN-PTCDI	628	1077	467	868
BNO-PTCDI	465	915	263	628
DD-PTCDI	169	549	127	566

enhanced intermolecular disorder, which in turn may also enhance the polaronic effect. As indeed indicated by the theoretical modeling,[16] at sufficiently high temperature (depending on materials), the polaronic effect can become more dominant than the energetic disorder in controlling the charge transport.

The activation energies shown in Table 1, particularly those obtained in the low-temperature range, are in good consistency with the values measured for the other organic semiconductors under similar temperatures using the FET devices under varying temperatures.[13,14,31] Also in the lower-temperature range, the activation energies of the two D−A PTCDIs, BN-PTCDI and BNO-PTCDI, are much higher than that of DD-PTCDI, which contains no donor moiety. This can be explained by the much increased disorder within the D−A materials, wherein intermolecular D−A interaction (concerted with the strong dipole−dipole interaction) would distort the molecular arrangement, creating traps for the charge carriers. In contrast, the DD-PTCDI material is mostly controlled by the $\pi-\pi$ stacking, for which there is little disorder contribution from the dipole−dipole interaction, considering the close to zero dipole moment of the symmetric molecule. When comparisons are made between BN-PTCDI and BNO-PTCDI in the low-temperature range, the activation energy of the former is significantly higher than the latter, ca. 1.35 and 1.77 times for the dark current and photocurrent measurement, respectively. The higher activation energy of BN-PTCDI is apparently due to the stronger D−A interaction between the phenylpiperidine group and PTCDI in comparison to that between phenylmorpholine and PTCDI in BNO-PTCDI material. Indeed, as indicated by our density-functional theory calculation (Figure S3), the electron-donating power (determined by the HOMO level) of phenylpiperidine is 0.13 eV stronger than that of the phenylmorpholine. It is interesting to note that with temperature increasing to sufficiently high levels (here around 80 °C), the relative difference in activation energy between the three nanofibers becomes much smaller than that observed in the low-temperature range. This implies that the thermally induced molecular disorder (e.g., conformational defects) at elevated temperature may override the effects of D−A or dipole−dipole interaction, which are usually dominant at low temperatures.

The enhanced low-temperature disorder of the two D−A PTCDI materials (compared to DD-PTCDI) as discussed above was also supported by the X-ray diffraction (XRD) and differential scanning calorimetry (DSC) measurements (Figures 3 and S4). Figure 3 shows the XRD patterns measured for BN-PTCDI, BNO-PTCDI, and DD-PTCDI nanofibers. For DD-PTCDI nanofibers, well-defined XRD peaks are observed and can be indexed from (001) to (007), which are consistent with the previous reports on the same fiber materials (though

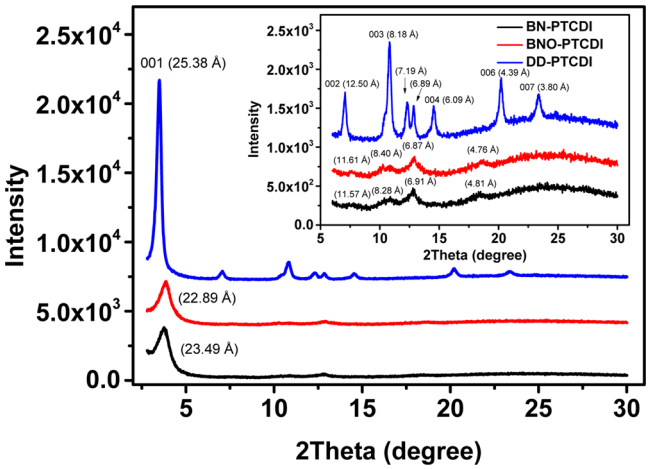

Figure 3. X-ray diffraction patterns of BN-PTCDI, BNO-PTCDI, and DD-PTCDI nanofibers. The inset is the enlarged spectrum in the degree range from 6° to 30°.

fabricated with slightly different self-assembly procedures).[30,32,33] The *d*-spacing of 25.38 Å (deduced from the primary peak at 3.49°) corresponds to the intercolumnar distance, which is about half of the length of two DD-PTCDI molecules tail-to-tail interdigitated.[34,35] The 23.37° peak is indexed as the cofacial stacking between two PTCDI planes, and the calculated stack spacing (3.80 Å) is consistent with the typical $\pi-\pi$ stacking distance as observed for other planar π-conjugated molecules.[33,34] To minimize the free energy caused by $\pi-\pi$ electronic repulsion, a transverse and/or longitudinal offset is usually observed between the stacked PTCDI planes, resulting in a different edge-to-edge distance from the $\pi-\pi$ stacking distance.[36] The *d*-spacing of 4.39 Å (calculated from the peak 20.21°) corresponds to the edge-to-edge distance between the two stacked DD-PTCDI planes, which take a tilted packing conformation. In contrast to the high-quality crystalline structure observed for DD-PTCDI, the structure of BN-PTCDI and BNO-PTCDI looks less organized as indicated by the XRD patterns in Figure 3. The XRD peak intensity measured for the nanofibers of BN-PTCDI and BNO-PTCDI decreased by about 1 order of magnitude in comparison to that of DD-PTCDI nanofibers. Nonetheless, the intercolumnar spacings, 23.49 and 22.89 Å, as calculated for BN-PTCDI and BNO-PTCDI from the primary diffraction peaks, are quite close to the spacing value (25.38 Å) obtained for DD-PTCDI, indicating a similar cofacial $\pi-\pi$ stacking arrangement drives the 1D growth of nanofibers in all three PTCDIs.

Consistent with the XRD measurement, the DSC result also suggests less ordered structure for the two D−A PTCDI materials compared to DD-PTCDI. DSC is a common method used for studying the phase transition of molecular materials, including the PTCDIs.[30,37,38] As shown in Figure S4, upon heating, DD-PTCDI nanofibers demonstrated three crystalline−crystalline transitions occurring at 85, 160, and 175 °C prior to the melting transition (T_m > 200 °C). When the sample was cooled, a dominant transition from mesophase to crystallization was observed at about 153 °C. Unlike DD-PTCDI, BN-PTCDI and BNO-PTCDI did not exhibit a clear phase transition upon heating, though during the cooling cycle a broad, asymmetric peak can be observed around 172 and 153 °C for BN-PTCDI and BNO-PTCDI, respectively, implying the transition from mesophase to crystallization phase. This

DOI: 10.1021/acs.jpclett.6b02639
J. Phys. Chem. Lett. 2017, 8, 292−298

observation suggests more disorder structure of the D−A PTCDIs compared to the highly organized molecular packing within DD-PTCDI. The high-quality crystalline structure of DD-PTCDI is mostly due to the symmetric molecular geometry substituted by two linear alkyl chains. This type of PTCDIs is conducive to forming organized columnar stacks in a manner similar to that of liquid crytals.[38] As discussed above, structure disorder leads to increased activation energy for charge transport, which is evidenced in our electrical current measurements shown in Figures 2 and S2. Such disorder-dependent thermoactivation was also observed previously by others in pentacene thin-film transistors,[15] for which the film morphologies could be tuned and optimized by deposition of the film on a substrate at varying temperatures. Depending on the deposition temperature, different quality of films can be obtained, and low-temperature deposition usually led to low-quality film with more deep level traps, which in turn resulted in large activation energy.

It is also interesting in Table 1 (Figure S2 as well) that the activation energy obtained particularly in the D−A PTCDI nanofibers was significantly decreased when measured under white light illumination in comparison to that in the dark. This decrease in activation energy is likely due to the increase in charge carrier density resulting from the photoinduced charge separation within the nanofibers. An increase in charge carrier density (here electrons for PTCDI) shifts up the Fermi level through the trap distribution, closer to the conduction band edge, and as a result, the thermal energy required to activate the trapped charge into hopping would be decreased. Such charge carrier density dependence of thermoactivation was evidenced or implied in other studies, both experimentally and theoretically, using the gate voltage to modulate the charge carrier density.[28,29]

The increase in charge carrier density upon illumination can be clearly seen from the dramatic increase in photocurrent compared to the dark current (Figure 2a,b). Indeed, the electrical current of the two D−A nanofibers, BN-PTCDI and BNO-PTCDI, was increased by more than 2 orders of magnitude when illuminated by white light. Such dramatic photoconductive enhancement is largely due to the photo-induced charge separation between the D moiety and PTCDI π-conjugated backbone (the A part), which produces increased density of charges.[27,34,39] The photocurrent response observed for DD-PTCDI under the same illumination condition was about 1 order of magnitude lower than that of the D−A PTCDIs, likely due to the lack of electron-donating groups. The photoinduced electron transfer from the D moieties to PTCDI is very thermodynamically favorable with a driving force of 0.74 and 0.61 eV for BN-PTCDI and BNO-PTCDI, respectively (Figure S3). The transferred electron will be delocalized along the $\pi-\pi$ stacks of PTCDIs, further enhancing the charge separation.[27] The photoinduced intramolecular electron transfer within the two D−A molecules was also evidenced by the efficient fluorescence quenching in both solutions and solid state (Figure 4 and S5). As shown in Figure 4, the BN-PTCDI and BNO-PTCDI molecules dissolved in chloroform exhibit very weak fluorescence emission, whereas DD-PTCDI demonstrated strong fluorescence under the same conditions. The dramatic fluorescence quenching is due to the efficient photoinduced intramolecular electron transfer from the D moiety to PTCDI (as illustrated in Figure S3). Similar fluorescence quenching has been observed within many other D−A molecules, including the PTCDIs substituted with

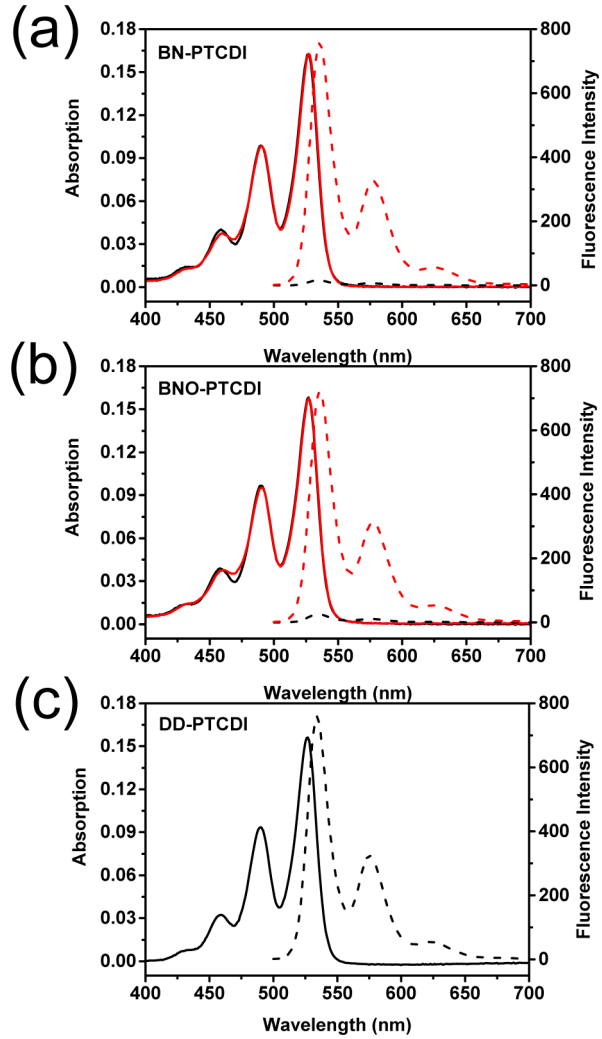

Figure 4. UV−vis absorption (black solid) and fluorescence (black dashed) spectra of (a) BN-PTCDI, (b) BNO-PTCDI, and (c) DD-PTCDI dissolved in chloroform (2 μmol L^{-1}). Under the same measurement conditions, the fluorescence intensities of BN-PTCDI and BNO-PTCDI solution were much lower than that of DD-PTCDI, but the quenched fluorescence could be recovered by addition of hydrochloric acid (0.1 mol L^{-1}), for which both the UV−vis absorption (red solid) and fluorescence (red dashed) spectra were then measured again under the same conditions.

different amines.[34,40] To further confirm the intramolecular electron transfer, hydrochloric acid was added into the solution of BN-PTCDI or BNO-PTCDI to protonate the amines, in order to lower the energy level of the lone electron pair, thus blocking the photoinduced intramolecular electron transfer as evidenced before in numerous D−A molecular systems.[34,40] Indeed, the addition of hydrochloric acid resulted in strong fluorescence turning on as shown in Figure 4. Similarly, the significant fluorescence quenching was also observed in the solid state of BN-PTCDI and BNO-PTCDI nanofibers, whereas DD-PTCDI nanofibers remained strongly fluorescent (Figure S5).

In conclusion, we have investigated the temperature-dependent charge transport (measured as electrical current) for three PTCDI nanofibers with two in D−A structure (BN-PTCDI and BNO-PTCDI) and a third one without strong donor substitution (DD-PTCDI). The results support the thermoactivated hopping mechanism for the charge transport,

DOI: 10.1021/acs.jpclett.6b02639
J. Phys. Chem. Lett. 2017, 8, 292−298

for which the activation energy was found to be primarily dependent on D−A structure. Indeed, both the D−A nanofibers showed activation energy that was significantly higher than that of the DD-PTCDI nanofibers for both the dark current and photocurrent measurements. D−A structure helps create disorder regarding both the charge-transfer and dipole−dipole interactions between stacked molecules, and the increased disorder enlarges the activation barrier. Significant increase in activation energy was found when heating the materials above the first crystallization to crystallization transition temperature, and this is likely due to the heating-enhanced intermolecular disorder, with which the polaronic effect may become more dominant in controlling the charge hopping process. Under visible light illumination, the electrical current of the nanofibers can be increased by orders of magnitude, thus providing the opportunity to examine the effect of charge carrier density on the activation energy of thermoactivated charge transport. As expected from the theoretical modeling in the literature, the increased charge carrier density caused a decrease in the activation energy because of the up-shifting of Fermi level through the energetic trap distribution in the bandgap. The photocurrent measurement offers an alternative way, in addition to the gate control in FET device, to modulate the charge carrier density in material and investigate the effect on the thermoactivation of charge hopping. This work also reveals a trade-off regarding the design rules of D−A molecular materials. On one hand, D−A structure enables charge transfer and separation, particularly under light illumination, producing high conductivity, but on the other hand, the D−A materials are often more disordered compared to the neutral (low dipole) materials, thus resulting in higher activation energy for charge transport. This may be conducive to developing more sensitive temperature sensors, but for many other electronic systems or applications more organized materials are usually required, which in turn demands more control of the intermolecular arrangement through molecular structural design and engineering.

■ ASSOCIATED CONTENT

Supporting Information

The Supporting Information is available free of charge on the ACS Publications website at DOI: 10.1021/acs.jpclett.6b02639.

Detailed experimental methods, electrical current profile of BN-PTCDI nanofibers in the dark with temperature variation, Arrhenius plot of current versus inverse temperature, schematic of calculated energy levels, DSC traces of PTCDI nanofibers, bright-filed and fluorescence optical microscopy images, and UV−vis absorption and fluorescence spectra of solid-state nanofibers (PDF)

■ AUTHOR INFORMATION

Corresponding Author

*E-mail: lzang@eng.utah.edu.

ORCID

Na Wu: 0000-0001-6322-6072

Notes

The authors declare no competing financial interest.

■ ACKNOWLEDGMENTS

This work was supported by the Department of Homeland Security, Science and Technology Directorate under Grant (2009-ST-108-LR0005), NSF (CBET 1502433).

■ REFERENCES

(1) Hains, A. W.; Liang, Z.; Woodhouse, M. A.; Gregg, B. A. Molecular Semiconductors in Organic Photovoltaic Cells. *Chem. Rev.* **2010**, *110*, 6689−6735.

(2) Coakley, K. M.; McGehee, M. D. Conjugated Polymer Photovoltaic Cells. *Chem. Mater.* **2004**, *16*, 4533−4542.

(3) Samuel, I. D. W.; Turnbull, G. A. Organic Semiconductor Lasers. *Chem. Rev.* **2007**, *107*, 1272−1295.

(4) Sirringhaus, H. Organic Semiconductors: An Equal-Opportunity Conductor. *Nat. Mater.* **2003**, *2*, 641−642.

(5) Jung, S.; Ji, T.; Varadan, V. K. Temperature Sensor Using Thermal Transport Properties in the Subthreshold Regime of an Organic Thin Film Transistor. *Appl. Phys. Lett.* **2007**, *90*, 062105.

(6) Ren, X.; Chan, P. K. L.; Lu, J.; Huang, B.; Leung, D. C. W. High Dynamic Range Organic Temperature Sensor. *Adv. Mater.* **2013**, *25*, 1291−1295.

(7) Trung, T. Q.; Ramasundaram, S.; Hong, S. W.; Lee, N.-E. Flexible and Transparent Nanocomposite of Reduced Graphene Oxide and P(VDF-TrFE) Copolymer for High Thermal Responsivity in a Field-Effect Transistor. *Adv. Funct. Mater.* **2014**, *24*, 3438−3445.

(8) Trung, T. Q.; Lee, N.-E. Flexible and Stretchable Physical Sensor Integrated Platforms for Wearable Human-Activity Monitoringand Personal Healthcare. *Adv. Mater.* **2016**, *28*, 4338−4372.

(9) Chortos, A.; Liu, J.; Bao, Z. Pursuing Prosthetic Electronic Skin. *Nat. Mater.* **2016**, *15*, 937−950.

(10) Someya, T.; Kato, Y.; Sekitani, T.; Iba, S.; Noguchi, Y.; Murase, Y.; Kawaguchi, H.; Sakurai, T. Conformable, Flexible, Large-Area Networks of Pressure and Thermal Sensors with Organic Transistor Active Matrixes. *Proc. Natl. Acad. Sci. U. S. A.* **2005**, *102*, 12321−12325.

(11) Lu, N.; Li, L.; Banerjee, W.; Sun, P.; Gao, N.; Liu, M. Charge Carrier Hopping Transport Based on Marcus Theory and Variable-Range Hopping Theory in Organic Semiconductors. *J. Appl. Phys.* **2015**, *118*, 045701.

(12) Tessler, N.; Preezant, Y.; Rappaport, N.; Roichman, Y. Charge Transport in Disordered Organic Materials and Its Relevance to Thin-Film Devices: A Tutorial Review. *Adv. Mater.* **2009**, *21*, 2741−2761.

(13) Coropceanu, V.; Cornil, J.; da Silva Filho, D. A.; Olivier, Y.; Silbey, R.; Brédas, J.-L. Charge Transport in Organic Semiconductors. *Chem. Rev.* **2007**, *107*, 926−952.

(14) Horowitz, G.; Hajlaoui, M. E.; Hajlaoui, R. Temperature and Gate Voltage Dependence of Hole Mobility in Polycrystalline Oligothiophene Thin Film Transistors. *J. Appl. Phys.* **2000**, *87*, 4456−4463.

(15) Knipp, D.; Street, R. A.; Völkel, A. R. Morphology and Electronic Transport of Polycrystalline Pentacene Thin-Film Transistors. *Appl. Phys. Lett.* **2003**, *82*, 3907−3909.

(16) Fishchuk, I. I.; Kadashchuk, A.; Hoffmann, S. T.; Athanasopoulos, S.; Genoe, J.; Bässler, H.; Köhler, A. Unified Description for Hopping Transport in Organic Semiconductors Including Both Energetic Disorder and Polaronic Contributions. *Phys. Rev. B: Condens. Matter Mater. Phys.* **2013**, *88*, 125202.

(17) Dieckmann, A.; Bässler, H.; Borsenberger, P. M. An Assessment of the Role of Dipoles on the Density-of-States Function of Disordered Molecular Solids. *J. Chem. Phys.* **1993**, *99*, 8136−8141.

(18) Dunlap, D. H.; Parris, P. E.; Kenkre, V. M. Charge-Dipole Model for the Universal Field Dependence of Mobilities in Molecularly Doped Polymers. *Phys. Rev. Lett.* **1996**, *77*, 542−545.

(19) Chang, J.-F.; Sirringhaus, H.; Giles, M.; Heeney, M.; McCulloch, I. Relative Importance of Polaron Activation and Disorder on Charge Transport in High-Mobility Conjugated Polymer Field-Effect Transistors. *Phys. Rev. B: Condens. Matter Mater. Phys.* **2007**, *76*, 205204.

DOI: 10.1021/acs.jpclett.6b02639
J. Phys. Chem. Lett. 2017, 8, 292−298

(20) Parris, P. E.; Kenkre, V. M.; Dunlap, D. H. Nature of Charge Carriers in Disordered Molecular Solids: Are Polarons Compatible with Observations? *Phys. Rev. Lett.* **2001**, *87*, 126601.
(21) Würthner, F.; Saha-Möller, C. R.; Fimmel, B.; Ogi, S.; Leowanawat, P.; Schmidt, D. Perylene Bisimide Dye Assemblies as Archetype Functional Supramolecular Materials. *Chem. Rev.* **2016**, *116*, 962−1052.
(22) Zang, L.; Che, Y.; Moore, J. S. One-Dimensional Self-Assembly of Planar π-Conjugated Molecules: Adaptable Building Blocks for Organic Nanodevices. *Acc. Chem. Res.* **2008**, *41*, 1596−1608.
(23) Chen, S.; Slattum, P.; Wang, C.; Zang, L. Self-Assembly of Perylene Imide Molecules into 1D Nanostructures: Methods, Morphologies, and Applications. *Chem. Rev.* **2015**, *115*, 11967−11998.
(24) Pasaogullari, N.; Icil, H.; Demuth, M. Symmetrical and Unsymmetrical Perylene Diimides: Their Synthesis, Photophysical and Electrochemical Properties. *Dyes Pigm.* **2006**, *69*, 118−127.
(25) Wu, N.; Wang, C.; Bunes, B. R.; Zhang, Y.; Slattum, P. M.; Yang, X.; Zang, L. Chemical Self-Doping of Organic Nanoribbons for High Conductivity and Potential Application as Chemiresistive Sensor. *ACS Appl. Mater. Interfaces* **2016**, *8*, 12360−12368.
(26) Huang, H.; Gross, D. E.; Yang, X.; Moore, J. S.; Zang, L. One-Step Surface Doping of Organic Nanofibers to Achieve High Dark Conductivity and Chemiresistor Sensing of Amines. *ACS Appl. Mater. Interfaces* **2013**, *5*, 7704−7708.
(27) Zang, L. Interfacial Donor−Acceptor Engineering of Nanofiber Materials to Achieve Photoconductivity and Applications. *Acc. Chem. Res.* **2015**, *48*, 2705−2714.
(28) Chesterfield, R. J.; McKeen, J. C.; Newman, C. R.; Ewbank, P. C.; da Silva Filho, D. A.; Brédas, J.-L.; Miller, L. L.; Mann, K. R.; Frisbie, C. D. Organic Thin Film Transistors Based on N-Alkyl Perylene Diimides: Charge Transport Kinetics as a Function of Gate Voltage and Temperature. *J. Phys. Chem. B* **2004**, *108*, 19281−19292.
(29) Fishchuk, I. I.; Kadashchuk, A. K.; Genoe, J.; Ullah, M.; Sitter, H.; Singh, T. B.; Sariciftci, N. S.; Bässler, H. Temperature Dependence of the Charge Carrier Mobility in Disordered Organic Semiconductors at Large Carrier Concentrations. *Phys. Rev. B: Condens. Matter Mater. Phys.* **2010**, *81*, 045202.
(30) Balakrishnan, K.; Datar, A.; Naddo, T.; Huang, J.; Oitker, R.; Yen, M.; Zhao, J.; Zang, L. Effect of Side-Chain Substituents on Self-Assembly of Perylene Diimide Molecules: Morphology Control. *J. Am. Chem. Soc.* **2006**, *128*, 7390−7398.
(31) Knipp, D.; Street, R. A.; Völkel, A.; Ho, J. Pentacene Thin Film Transistors on Inorganic Dielectrics: Morphology, Structural Properties, and Electronic Transport. *J. Appl. Phys.* **2003**, *93*, 347−355.
(32) Huang, Y.; Fu, L.; Zou, W.; Zhang, F.; Wei, Z. Ammonia Sensory Properties Based on Single-Crystalline Micro/Nanostructures of Perylenediimide Derivatives: Core-Substituted Effect. *J. Phys. Chem. C* **2011**, *115*, 10399−10404.
(33) Jones, B. A.; Facchetti, A.; Wasielewski, M. R.; Marks, T. J. Tuning Orbital Energetics in Arylene Diimide Semiconductors. Materials Design for Ambient Stability of n-Type Charge Transport. *J. Am. Chem. Soc.* **2007**, *129*, 15259−15278.
(34) Che, Y.; Yang, X.; Liu, G.; Yu, C.; Ji, H.; Zuo, J.; Zhao, J.; Zang, L. Ultrathin n-Type Organic Nanoribbons with High Photoconductivity and Application in Optoelectronic Vapor Sensing of Explosives. *J. Am. Chem. Soc.* **2010**, *132*, 5743−5750.
(35) Bushey, M. L.; Hwang, A.; Stephens, P. W.; Nuckolls, C. Enforced Stacking in Crowded Arenes. *J. Am. Chem. Soc.* **2001**, *123*, 8157−8158.
(36) Wurthner, F. Perylene Bisimide Dyes as Versatile Building Blocks for Functional Supramolecular Architectures. *Chem. Commun.* **2004**, 1564−1579.
(37) Cormier, R. A.; Gregg, B. A. Synthesis and Characterization of Liquid Crystalline Perylene Diimides. *Chem. Mater.* **1998**, *10*, 1309−1319.
(38) Struijk, C. W.; Sieval, A. B.; Dakhorst, J. E. J.; van Dijk, M.; Kimkes, P.; Koehorst, R. B. M.; Donker, H.; Schaafsma, T. J.; Picken, S. J.; van de Craats, A. M.; et al. Liquid Crystalline Perylene Diimides: Architecture and Charge Carrier Mobilities. *J. Am. Chem. Soc.* **2000**, *122*, 11057−11066.
(39) Rühle, V.; Lukyanov, A.; May, F.; Schrader, M.; Vehoff, T.; Kirkpatrick, J.; Baumeier, B.; Andrienko, D. Microscopic Simulations of Charge Transport in Disordered Organic Semiconductors. *J. Chem. Theory Comput.* **2011**, *7*, 3335−3345.
(40) Zang, L.; Liu, R.; Holman, M. W.; Nguyen, K. T.; Adams, D. M. A Single-Molecule Probe Based on Intramolecular Electron Transfer. *J. Am. Chem. Soc.* **2002**, *124*, 10640−10641.

DOI: 10.1021/acs.jpclett.6b02639
J. Phys. Chem. Lett. 2017, 8, 292−298